Theoretical Studies on Excited States of a Phenolate Anion in the Environment of Photoactive Yellow Protein

Zhi He,[†] Charles H. Martin,[‡] Robert Birge,[§] and Karl F. Freed*[,†]

The James Franck Institute and the Department of Chemistry, The University of Chicago, Chicago, Illinois 60637, Quantum Theory Project and Department of Chemistry, University of Florida, Gainesville, Florida 32606, and W. K. Keck Center for Molecular Electronics and the Department of Chemistry, Syracuse University, Syracuse, New York 13244

Received: July 27, 1999; In Final Form: December 23, 1999

In an effort to understand the dynamical process in the photocycle of photoactive yellow protein (PYP), we perform ab initio effective valence shell Hamiltonian (H^v) calculations for the low-lying excited states in two simple models of the PYP chromophore: (i) a phenolate anion surrounded by seven charged amino acids, which are modeled as point charges and (ii) to consider the effect of hydrogen bonding of the Try 42 and Glu 46 residues, a phenolate anion with two hydrogen-bonded water molecules embedded in the same point-charge field as in the previous model. Second-order H^v calculations for the isolated phenolate anion are in good agreement with calculations using the EOM-CCSD and sa-CASMP2 methods, while the hydrogen bonds exert a minor influence for the lower excited states of the phenolate anion in the environment of the PYP chromophore. The electrostatic enviroment of PYP provides the dominant stablization to shift the lowest singlet excited state below the lowest ionization potential. Comparisons between different advanced ab initio methods imply that second-order H^v calculations can provide sufficiently accurate spectral data for biological chromophores in their native environments. This feature is significant because the second-order H^v method is much easier and of lower computational cost to implement than other high level approaches, such as the MRCCSD, EOM-CCSD, and sa-CASMP2 methods. Additionally, we also discuss the hydrogen-bonding interactions between the phenolate anion and the PYP and analyze the charge distributions for the full chromophore in PYP.

I. Introduction

The photoactive yellow protein (PYP) is a small soluble protein found in the halophilic bacterium *Ectothiorhodospira-halophila*.[1] PYP is a light sensor that, presumably, mediates the negatively phototactic response to intense blue light in certain halophilic bacteria. On absorbing light, PYP undergoes a series of spectral changes, owing to the formation of red-shifted and blue-shifted intermediates, and then returns to the dark state.[2−5] This photocycle involves the trans → cis isomerization of the chromophore[6] and is thus very similar to that of bacteriorhopdopsin (BR). Therefore, studies of PYP are not only of intrinsic interest, but also are useful to elucidate many controversial and/or mysterious features concerning the behavior of other visual pigments, such as the rhodopsins (RH) and BR.

While numerous theoretical studies exist for BR, BR is a membrane bound protein, and the only structural information available comes from poorly resolved electron-cryo microscopy. Detailed studies of the rhodopsins fare even worse, being based on even cruder structures determined from homology modeling of BR. In contrast to BR and RH, the three-dimensional structure of PYP is known to very high resolution.[7] Recently, experimental PYP structures of photocycle intermediates have also been reported.[8−9] The elucidation of the three-dimensional structures of PYP at atomic resolution encourages efforts to perform theoretical and computational studies for PYP to understand the dynamic process in the photocycle of the PYP.

Since the long time dynamics of PYP are driven by the photoisomerization process, a complete theoretical model requires detailed knowledge of the potential energy surfaces for the excited electronic states of the anion of the protein bound *para*-coumaric acid ($O^--(C_6H_4)-(CH)=(CH)-(CO)-S-$protein), which is the photoactive chromophore of PYP, a negative ion that sits embedded in a charged protein pocket. Upon light absorption, the anion of *para*-coumaric acid is believed to isomerize about the free C=C bond, initiating a series of complex and long time protein motions. The exact photoisomerization process remains poorly understood as do factors which regulate the absorption spectra.

In an effort to assist predictions of the long time dynamics of PYP, we seek to understand how to treat the electronic spectra and excited-state potential energy surfaces for the anion of *para*-coumaric acid. It is readily possible to employ semiempirical calculations for the excited states to describe the spectra and excited-state potential energy surfaces of *para*-coumaric acid. Because semiempirical model Hamiltonians include some degree of electron−electron correlation, the semiempirical calculations might yield the correct anion ground states, and low-lying excitation energies may perform well near the ground state equilibrium geometries. However, it still remains controversial whether semiempirical methods can provide highly accurate excited states potential energy surfaces for the isomerization reaction and for the hydrogen bond network in PYP. On the other hand, owing to computational limitations, it is not yet

* Corresponding author.
† The James Franck Institute and the Department of Chemistry.
‡ Quantum Theory Project and Department of Chemistry.
§ W. K. Keck Center for Molecular Electronics and the Department of Chemistry.

10.1021/jp992615s CCC: $19.00
Published on Web 03/09/2000

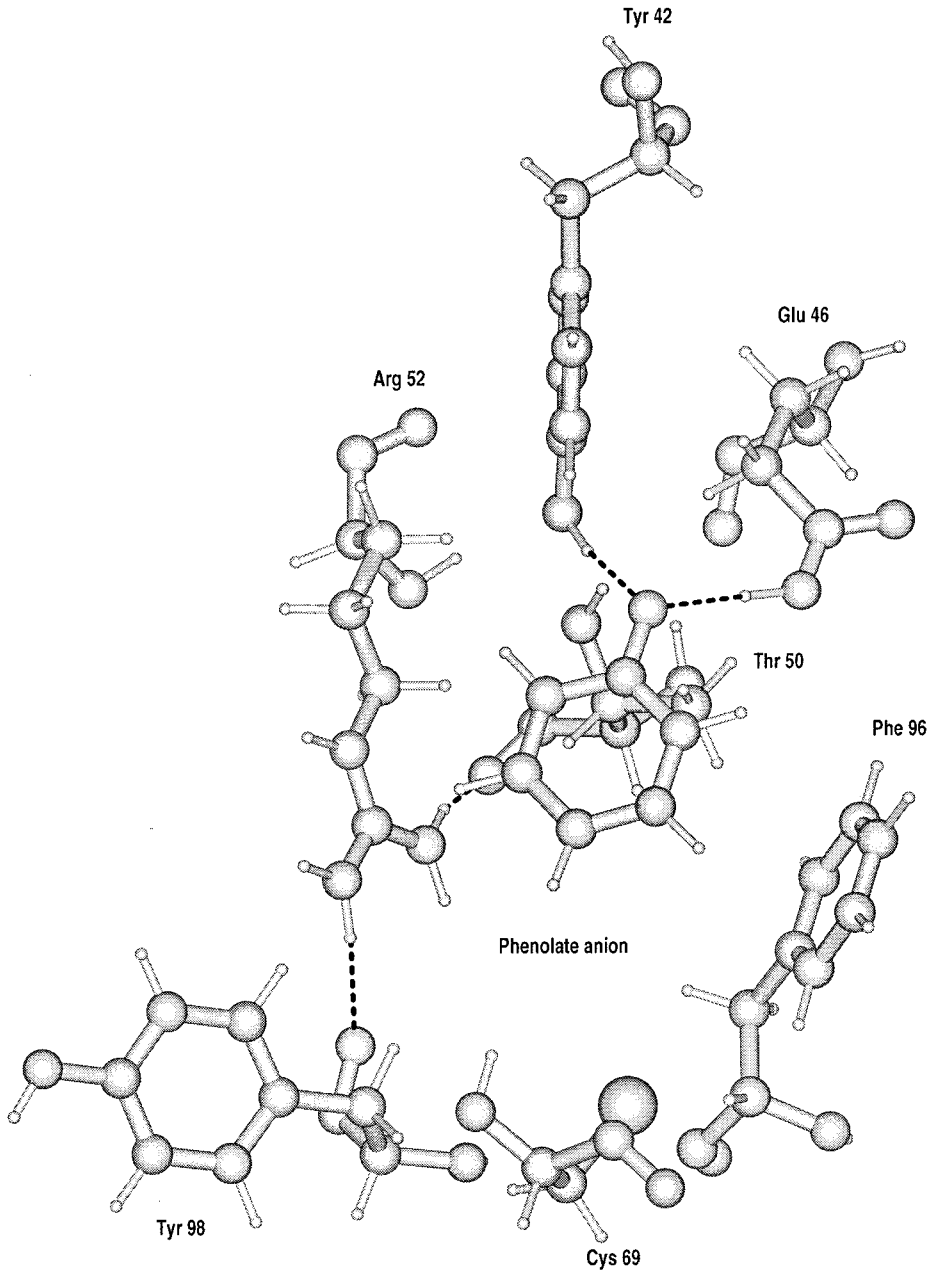

Figure 1. Simple model used for the PYP chromophore: A phenolate anion is surrounded by seven amino acids. Dashed lines denote strong hydrogen bonds.

possible to perform accurate ab initio calculations for the whole protein of PYP. Hence, it is necessary to study ab initio calculations for simple models of PYP.

As an initial simplification, we model the chromophore in a realistic protein environment as a phenolate anion surrounded by seven amino acids which, in turn, are modeled as point charges: a protein-bound phenolate anion (see Figure 1). This point-charge field simulates the electrostatic chromophore environment, which stabilizes the ground and low-lying excited states of the phenolate anion. Such a model is readily amenable to high-level ab initio calculations. However, the anion is also well-known to be stabilized by the nearby Tyr 42 and Glu 46 groups through two hydrogen bonds. One hydrogen bond exists between the phenolic oxygen of the chromophore and the hydroxyl group of Tyr 42, while the other involves the protonated carboxyl of Glu 46. Because charge transfer may occur between the phenolate anion and the surrounding amino acids, the simplest PYP−chromophore model of the protein-bound phenolate anion is improved by including a portion of the surrounding amino acid binding sites in the ab initio calculations. Thus, we also perform the calculations for a complex of the protein-bound phenolate anion with two hydrogen-bonded water molecules at the positions where the Tyr 42 and Glu 46 residues have hydrogen bonds in PYP.

The present paper studies the low-lying excited states of the phenolate anion in the PYP environment by calculating the excitation energies for the protein-bound phenolate anion and the protein-bound phenolate anion$-2H_2O$ complex with the high-level ab initio effective valence shell Hamiltonian method.[10−14] A subsequent work will consider the effects of the electrostatic environment surrounding the chromophore in PYP and of the hydrogen bonds between the chromophore and its adjoining amino acids.

The next section describes the ab initio H^v theory in second order. The description of the theory is designed, in part, to elucidate the information required for second-order calculations and their relative computational simplicity compared to all the other methods considered (except, of course, CIS). Those readers

uninterested in the theoretical details may skip to section III where we describe the H^v calculations for an isolated phenolate anion and the construction of the two simplified models for the chromophore in PYP. Section IV compares the H^v results with other calculations, such as the equation-of-motion coupled-cluster method with the restriction to all single and double excitations (EOM-CCSD),[15−17] the state-average complete active space SCF method (sa-CASSCF)[18,19] and its second-order correlation correction extension (sa-CASMP2),[20] and the single-excitation configuration interaction approach (CIS).[21−24] We also discuss the hydrogen-bonding interactions in PYP and analyze the charge distributions for the chromophore in PYP.

II. Theory

Perturbation theory precedes by decomposing the Hamiltonian (H) for a system into the zeroth order Hamiltonian (H_0) and the perturbation (V),

$$H = H_0 + V \tag{1}$$

In general, the zeroth-order Hamiltonian H_0 should be a reasonable approximation to the full Hamiltonian H and should be simple enough to manage. To satisfy these and other constraints, the effective valence shell Hamiltonian (H^v) approach[10−14] uses a quite general diagonal one-electron form of H_0 defined by

$$H_0 = \sum_c \epsilon_c a_c^\dagger a_c + \sum_v \epsilon_v a^\dagger{}_v a_v + \sum_e \epsilon_e a^\dagger{}_e a_e \tag{2}$$

where the set of one-electron orbitals is partitioned into core, valence, and excited orbitals. The symbols $a_c^\dagger(a_c)$, $a_v^\dagger(a_v)$, and $a_e^\dagger(a_e)$ in equation 2 are creation (annihilation) operators for core (c), valence (v), and excited orbitals (e), while ϵ_c, ϵ_v, and ϵ_e, are, respectively, the corresponding core, valence, and excited orbital energies. The following also uses the subscript u to denote valence spin−orbitals that are occupied in a given reference state Φ_k, while w denotes virtual, i.e., unoccupied, valence orbitals in state Φ_k. An advantage to the partitioning of H as in eqs 1 and 2 is to permit the orbital and orbital energies to be chosen independent of each other in order to optimize the convergence properties of the perturbation expansion. Forcing degeneracy of the valence orbitals often eliminates the occurrence of detrimentally small perturbation energy denominators, thereby improving the convergence of the perturbation expansion.[25] For this reason, when the valence spaces are large, we usually prefer to introduce an averaged valence shell orbital energy, i.e., eq 2 is rewritten as

$$H_0 = \sum_c \epsilon_c a_c^\dagger a_c + \bar{\epsilon}_v \sum_v a_v^\dagger a_v + \sum_e \epsilon_e a_e^\dagger a_e \tag{3}$$

Because the choice of orbitals clearly affects the perturbative convergence, the H^v method seeks improved accuracy and convergence of the calculations by using improved virtual orbitals (IVOs) (defined as eigenfunctions of the ground-state Fock operator with one electron removed) and by taking the appropriate orbital energies.

Next, the exact Hamiltonian H for the valence states is transformed into one involving an effective valence shell Hamiltonian H^v, which is diagonalized solely within the reference space (also called the valence space) to yield all reference space state energies simultaneously from a single calculation. There are numerous ways to derive a theoretical expression for the exact H^v. Here we exploit generalized quasidegenerate many-body perturbation theory, where an expression for the Hermitian H^v through third order is represented by

$$\begin{aligned} H^v = PHP &+ \frac{1}{2}[\sum_k PVQ(E_k^0 - H_0)^{-1}QV|\Phi_k\rangle\langle\Phi_k| + \text{hc}] \\ &+ \frac{1}{2}[\sum_k PVQ(E_k^0 - H_0)^{-1}\text{QVQ}(E_k^0 - H_0)^{-1}QV \\ &\qquad |\Phi_k\rangle\langle\Phi_k| + \text{hc} \\ &- \sum_{k,k'} PVQ(E_k^0 - H_0)^{-1}Q(E_{k'}^0 - H_0)^{-1}QV|\Phi_{k'}\rangle \times \\ &\qquad \langle\Phi_{k'}|V|\Phi_k\rangle\langle\Phi_k| \\ &+ \text{hc}] + \ldots \end{aligned} \tag{4}$$

where hc denotes the Hermitian conjugation of the preceding term, and P and Q are, respectively, projection operators onto the valence and excited spaces,

$$P = \sum_k |\Phi_k\rangle\langle\Phi_k| \tag{5}$$

and

$$Q = 1 - P \tag{6}$$

with $\{\Phi_k\}$ the zeroth-order reference states which are taken here as having no core holes and/or electrons occupying excited orbitals. Thus, the valence space is complete. Consequently, it follows that

$$PH_0P = \sum_k E_k^0 |\Phi_k\rangle\langle\Phi_k| \tag{7}$$

with E_k^0 given by

$$E_k^0 = \sum_c \epsilon_c + \sum_u \epsilon_u \tag{8}$$

Simple single-reference perturbation theory employs a single determinantal reference function Φ_0, whereupon the operator Q_1 is uniquely specified by

$$Q_1 = \sum_{n=1}^{\infty} \sum_{i_1<\ldots<i_n} \sum_{a_1<\ldots<a_n} |\Phi_{i_1\ldots i_n}^{a_1\ldots a_n}\rangle\langle\Phi_{i_1\ldots i_n}^{a_1\ldots a_n}| \tag{9}$$

where the indices a_m and i_m ($m = 1, \ldots, n$) and the summations run, respectively, over all virtual and occupied spin−orbitals in Φ_0. However, in the multireference valence space, a clear separation is no longer possible between the particle and hole states, since the spin-orbitals occupied in one zeroth-order valence state may be empty in another. The analogue of eq 9 for Q is, hence, more complicated,

$$Q = \sum_{n=1}^{\infty} \sum_{i_1<\ldots<i_n} \sum_{a_1<\ldots<a_n} |\Phi_{i_1\ldots i_n}^{a_1\ldots a_n}(k)\rangle\langle\Phi_{i_1\ldots i_n}^{a_1\ldots a_n}(k)| \tag{10}$$

The ranges of the summations over a_m and i_m do not overlap and are strictly defined by the determinant Φ_k, i.e., $i_1, \ldots, i_n$ are summed over levels occupied in Φ_k, and $a_1, \ldots, a_n$ run over levels unoccupied in Φ_k with the provision that all the $\{a_m, i_m\}$ cannot simultaneously be valence orbitals. Then, using eqs 8 and 10 produces the matrix elements of second-order $H_{2\text{nd}}^v$ of eq 4 in the form

$$\langle\Phi_{k'}|H^{v}_{2nd}|\Phi_k\rangle = \frac{1}{2}[\langle\Phi_{k'}|VQ(E^0_k - H_0)^{-1}QV|\Phi_k\rangle + \text{hc}] \quad (11)$$

$$= \frac{1}{2}[\sum_{i,a}\langle\Phi_{k'}|V|\Phi^a_i(k)\rangle a^a_i(k) + a^a_i(k')\langle\Phi^a_i(k')|V|\Phi_k\rangle] + \frac{1}{8}\sum_{i_1,i_2}\sum_{a_1,a_2}[\langle\Phi_{k'}|V|\Phi^{a_1a_2}_{i_1i_2}(k)\rangle a^{a_1a_2}_{i_1i_2}(k) + a^{a_1a_2}_{i_1i_2}(k')\langle\Phi^{a_1a_2}_{i_1i_2}(k')|V|\Phi_k\rangle] \quad (12)$$

where the amplitudes are given by

$$a^a_i(k) = \frac{\langle\Phi^a_i(k)|V|\Phi_k\rangle}{\epsilon_i - \epsilon_a} \quad (13)$$

$$= \frac{h^0_{ai}}{\epsilon_i - \epsilon_a} \quad (14)$$

$$a^{a_1a_2}_{i_1i_2}(k) = \frac{\langle\Phi a^{a_1a_2}_{i_1i_2}(k)|V|\Phi_k\rangle}{\epsilon_{i_1} + \epsilon_{i_2} - \epsilon_{a_1} - \epsilon_{a_2}} \quad (15)$$

$$= \frac{\tilde{V}_{a_1a_2,i_1i_2}}{\epsilon_{i_1} + \epsilon_{i_2} - \epsilon_{a_1} - \epsilon_{a_2}} \quad (16)$$

$$(\tilde{V}_{a_1a_2,i_1i_2} = V_{a_1a_2,i_1i_2} - V_{a_1a_2,i_2i_1})$$

Equations 14 and 16 use the second quantized notation for V,

$$V = \sum_{pq} h^0_{pq}\, a^\dagger_p a_q + \frac{1}{2}\sum_{pq}\sum_{rs} V_{pq,rs} a^\dagger_p\, a^\dagger_q a_s a_r \quad (17)$$

where the one-electron portion is

$$h^0_{pq} \equiv h_{pq} - \delta_{pq}\epsilon_p \quad (18)$$

and h_{pq} and $V_{pq,rs}$ are the usual one-electron (i.e., electronic kinetic energy plus nuclear−electron attraction) matrix elements between general spin-orbitals p and q and the two-electron repulsion integrals, respectively. The single- (double)-excitation amplitudes $a^a_i(k)$ ($a^{a_1a_2}_{i_1i_2}(k)$) in eq (14) [eq 16] can further be separated into three (eight) classes: $a^\alpha_c(k)$ ($\alpha = e$ and w), $a^e_u(k)$, and $a^w_c(k)$ ($a^{\alpha\alpha'}_{cc'}(k)$, $a^{\alpha e}_{cu}(k)$, $a^{\alpha w}_{cc'}(k)$, $a^{ee'}_{uu'}(k)$, $a^{\alpha w}_{cu}(k)$, $a^{ww'}_{cc'}(k)$, $a^{we}_{uu'}(k)$, and $a^{ww'}_{uc}(k)$). Therefore, considering these different types of single and double amplitudes in eq 12, a computable form of the H^{v}_{2nd} emerges as

$$H^{v}_{2nd} = \sum_{k,k'}|\Phi_{k'}\rangle\langle\Phi_{k'}|H^{v}_{2nd}|\Phi_k\rangle\langle\Phi_k| \quad (19)$$

$$= \sum_{c\alpha} h^0_{c\alpha}\, a^\alpha_c + \frac{1}{4}\sum_{cc',\alpha\alpha'}\tilde{V}_{cc',\alpha\alpha'}a^{\alpha\alpha'}_{cc'} + \sum_{w,u}\tilde{u}^{(2)}_{w,u}\, a^\dagger_w a_u + \frac{1}{(2!)^2}\sum_{ww',uu'}\tilde{v}^{(2)}_{ww',uu'}\, a^\dagger_w\, a^\dagger_{w'}a_{u'}a_u + \frac{1}{(3!)^2}\sum_{ww'w'',uu'u''}\tilde{w}^{(2)}_{ww'w'',uu'u''}\, a^\dagger_w\, a^\dagger_{w'}\, a^\dagger_{w''}a_{u''}a_{u'}a_u \quad (20)$$

where the ab initio effective H^v integrals (also called the true parameters) $\tilde{u}^{(2)}_{w,u}$, $\tilde{v}^{(2)}_{ww',uu'}$, and $\tilde{w}^{(2)}_{ww'w'',uu'u''}$ are determined by

$$\tilde{u}^{(2)}_{w,u} = \frac{1}{2}\Big[\sum_e(h^0_{we}\,a^e_u + a^e_w\,h^0_{eu}) - \sum_c(h^0_{cu}\,a^w_c + a^u_c\,h^0_{wc}) + \sum_{c\alpha}(\tilde{V}_{cw,\alpha u}a^\alpha_c + a^{\alpha u}_{cw}\,h^0_{\alpha c}) + \sum_{c\alpha}(h^0_{c\alpha}\,a^{\alpha w}_{cu} + a^\alpha_c\,\tilde{V}_{\alpha w,cu}) + \sum_{c\alpha,e}(\tilde{V}_{cw,\alpha e}a^{\alpha e}_{cu} + a^{\alpha e}_{cw}\tilde{V}_{\alpha e,cu}) - \frac{1}{2}\sum_{cc',\alpha}(\tilde{V}_{cc',\alpha u}a^{\alpha w}_{cc'} + a^{\alpha u}_{cc'}\tilde{V}_{\alpha w,cc'})\Big] \quad (21)$$

$$\tilde{v}^{(2)}{}_{ww',uu'} = \frac{1}{2}\sum_P(-1)^P P(u/u')[\sum_e(\tilde{V}_{ww',eu'}a^e_u + a^{eu'}_{ww'}\,h^0_{eu}) - \sum_c(h^0_{cu'}\,a^{ww'}_{uc} + a^{u'}_c\tilde{V}_{ww',uc})] + \frac{1}{2}\sum_P(-1)^P P(w/w')[\sum_e(h^0_{we}\,a^{ew'}_{uu'} + a^e_w\tilde{V}_{ew',uu'}) - \sum_c(\tilde{V}_{cw',uu'}a^w_c + a^{uu'}_{cw'}\,h^0_{wc})] + \frac{1}{4}[\sum_{ee'}(\tilde{V}_{ww',ee'}a^{ee'}_{uu'} + a^{ee'}_{ww'}\,\tilde{V}_{ee',uu'}) + \sum_{cc'}(\tilde{V}_{cc',uu'}a^{ww'}_{cc'} + a^{ww'}_{cc'}\,\tilde{V}_{ww',cc'})] + \frac{1}{2}\sum_P(-1)^P P(u/u'|w/w')\sum_{c\alpha}(\tilde{V}_{cw',\alpha u'}a^{\alpha w}_{cu} + a^{\alpha u'}_{cw'}\,\tilde{V}_{\alpha w,cu}) \quad (22)$$

and

$$\tilde{w}^{(2)}_{ww'w'',uu'u''} = \frac{1}{2}\sum_P(-1)^P P(u/u'u''|w/w'w'')[\sum_e(\tilde{V}_{w'w'',eu}a^{ew}_{u''u'} + a^{ew}_{w'w''}\tilde{V}_{ew,u''u'}) - \sum_c(\tilde{V}_{cw,u''u'}a^{w'w''}_{cu} + a^{u''u'}_{cw}\tilde{V}_{w'w'',cu})] \quad (23)$$

The permutation symbol $\sum_P(-1)^P P(u/u'|w/w')$ implies a summation over the identity permutation, all permutations that interchange the orbital label u with u', and all permutations of w with w'. The operation $\sum_P(-1)^P P(u/u'u''|w/w'w'')$ involves interchanges of u with u' or u'' and of w with w' or w'' but no permutation of the form $u' \leftrightarrow u''$ or $w' \leftrightarrow w''$. Comparing the various terms in eqs 21−23, the most time-consuming step in the second-order H^{v}_{2nd} calculation is the evaluation of the first part in eq 23, which involves asymptotically $n^3_{occ\_val}\, n^3_{virt\_val}\, N_{exci}$ operations where N_{exci} is the number of excited orbitals. However, the number of occupied (or virtual) valence orbitals n_{occ_val} (or n_{virt_val}) is usually not more than 4. Hence, the H^{v}_{2nd} method offers significant time savings over the multireference couple−cluster method with single and double excitations (MRCCSD)[26] or even over the EOM-CCSD approach. Moreover, the following sections demonstrate that the present H^{v}_{2nd} results agree nicely with EOM-CCSD (or sa-CASMP2) computations for the low-lying excited states of the phenolate anion. The H^{v}_{2nd} treatment requires the same integral set as in the CASMP2 approach,[27] but there is no need for the lengthy and often difficult state averaged CASSCF procedure. Note that eqs 21−23 contain excitations out of core orbitals, a feature that enables relegating weakly correlating orbitals to the core.

A similar appproach may also be applied to obtain the third-order H^{v}_{3rd} expression analogous to eq 20, but with the difference that four electron effective intergals $\tilde{x}^{(3)}_{ww'w''w''',uu'u''u'''}$ now appear in third order. The H^{v}_{3rd} "true parameters" $\tilde{u}^{(3)}_{w,u}$, $\tilde{v}^{(3)}_{ww',uu'}$, $\tilde{w}^{(3)}_{ww'w'',uu'u''}$, and $\tilde{x}^{(3)}_{ww'w''w''',uu'u''u'''}$ can also be determined in terms of a^{a}_{i} and $a^{a_1a_2}_{i_1i_2}$, or alternatively by means of diagrams.[12] Presently, H^{v}_{3rd} computations are quite computer intensive, so it is describable to study modifications requiring only a second-order treatment.[25,28]

Using the above derivation, we can directly compare the H^{v} approach with the similar equations in the multireference coupled cluster (MRCCSD) approach.[26] Such a comparison shows that the H^{v} method does not require as large a set of amplitudes as in the MRCCSD approach. Thus, the second-order H^{v} treatment is much simpler to implement computationally than MRCCSD, and second-order H^{v} calculations may readily be applied for large systems. The H^{v} method seeks to use rather large reference spaces (the largest used here contains 1225 configurations) and low order perburbative truncations, while MRCCSD is limited to rather small reference spaces but retains some contributions to infinite orders. Moreover, the ability of choosing the orbitals and orbital energies independently introduces possible avenues for producing faster convergence of the H^{v} expansion in low orders to yield accurate spectral data for large systems.

III. Computational Details

The H^{v} calculations are usually performed in three steps: (i) generation of valence orbitals and orbital energies, (ii) calculation of the true parameters $\tilde{u}_{w,u}$, $\tilde{v}_{ww',uu'}$, etc., and (iii) diagonalization of H^{v} in the valence space to obtain the desired valence state energies. A single H^{v} calculation provides all vertical excitation energies simultaneously for a given system.

A. The Isolated Phenolate Anion. This subsection simply describes H^{v} calculations for an isolated phenolate anion, while their comparison with calculations using the EOM-CCSD, sa-CASSCF, sa-CASMP2, and CIS approaches are given in section IV. These comparisons are useful to assess the accuracy of various alternatives available within the H^{v} formulation. Because the excitation energies exceed the electron affinity of the phenolate anion (see below), the excited states of the isolated anion are Feshbach resonances which correspond to quasibound (i.e., temporary, decaying autoionizing) states lying in the ionization continuum. These excited anion Feshbach resonances can be treated by the H^{v} method.[29] Although the other approaches have not, to our knowledge, been tested for treating anion Feshbach resonances, the absence of diffuse functions in the 4-31G basis should lead to comparable qualities for these quasibound states and thereby make the comparisons meaningful. The computations (see next section) indeed yield very similar descriptions for all low-lying states.

The optimized geometry of the isolated phenolate anion has been determined using restricted Hartree−Fock (RHF) computations, the standard 4-31G basis set, and C_s symmetry. The geometry optimization for the isolated anion and for the phenolate anion in the PYP environment in next subsection are all performed with the Gaussian 94 program package.[20] Figure 2 presents the calculated structural parameters for the isolated phenolate anion, where bond distances are given in angstroms and angles in degrees. The optimized structure is quite close to the geometry previously optimized by Nwobi et al. with RHF/6-311++G(2d,p) computations,[30] and it is also similar to the X-ray structure in PYP.[7] The major difference between the optimized geometry and the protein-bound structure appears in the bond angle $\angle C_3C_4C_5$ in Figure 2, which differs by about 7° between the two structures. Obviously, the optimized phenolate anion geometry possesses higher C_{2v} symmetry, which is destroyed in the protein-bound system.

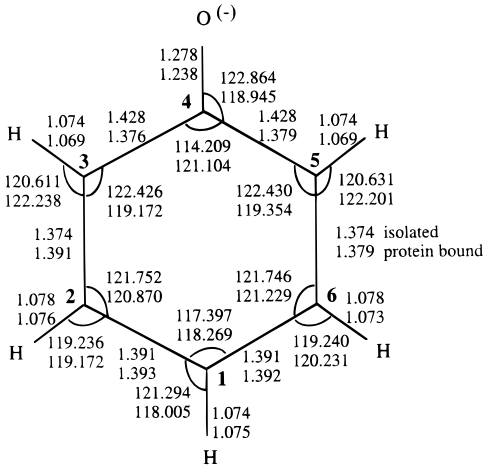

Figure 2. Schematic decription of structural parameters for the isolated (upper numbers) and protein-bound (lower numbers) phenolate anion.

The H^{v} calculations are performed with a valence space containing seven orbitals (labeled as 7V) using 4-31G and 6-31G* basis sets. Ground-state HF calculations provide the core and the four "occupied" valence orbitals (1π, 2π, 3π, and 4π) along with all of their orbital energies. To define the remaining three π "virtual" valence orbitals, (5π, 6π, 7π), we use frozen orbital SCF/MCSCF calculations, also called IVO/MCSCF calculations, in which each step involves the optimization of a single virtual orbital for the H^{v} valence space. The virtual valence orbitals and their orbital energies are obtained from the following set of open-shell triplet SCF calculations where only the single orbital outside the square brackets is varied:

$$[(1\pi)^2(2\pi)^2(3\pi)^1(4\pi)^2](5\pi^*)^1$$

$$[(1\pi)^1(2\pi)^2(3\pi)^2(4\pi)^2(5\pi^*)^0](6\pi^*)^1$$

$$[(1\pi)^2(2\pi)^2(3\pi)^1(4\pi)^2(5\pi^*)^0(6\pi^*)^0](7\pi^*)^1$$

A final step produces the excited orbitals by diagonalizing the ground-state Fock operator in the orbital space orthogonal to all core and valence orbitals. The IVOs procedures are clearly more appropriate to describing low-lying excited states than the V^N SCF virtual orbitals. Moreover, the IVO orbital energies are lower and improve the quasidegeneracy of the valence space. These diminished IVO energies can improve the low order convergence of the H^{v} energies.

Table 1 presents all H^{v} valence orbital energies. The IVO energies are 0.24−0.31 au lower than the corresponding ground-state SCF virtual orbital energies. Table 2 summarizes the first-, second-, and third-order H^{v} excitation energies for the isolated phenolate anion as computed with the two basis sets (4-31G and 6-31G*). Both singlet and triplet states are considered here, although the excited singlet states are most important for study of the initial stage of PYP's photocycle. Only a rather small decrease (by 0.0093−0.2369 eV) appears in the excitation energies for singlet and triplet states in both the second- and third-order H^{v} calculations as the 4-31G basis set is extended to the 6-31G* basis set (except the 2 ^{3}A state where the H^{v}_{3rd}/6-31G* energy is slightly higher by 0.0186 eV than the

TABLE 1: Comparison of Valence Orbital Energies (au) for the Isolated, Protein-Bound Phenolate Anion and for the Protein-Bound Phenolate Anion−$2H_2O$ Complex with the 4-31G Basis Set[a]

orbitals	isolated 4-31G	anion 6-31G*	bound anion	bound anion−$2H_2O$ complex
RHF	−304.531 122	−304.967 705	−310.308 826	−460.974 741
1π	−0.338 985	−0.332 797	−0.492 383	−0.509 691
2π	−0.247 827	−0.246 968	−0.394 189	−0.411 421
3π	−0.164 314	−0.159 676	−0.287 086	−0.299 208
4π	−0.065 692	−0.066 931	−0.209 376	−0.229 501
5π	0.335 064	0.333 685	0.203 812	0.190 405
6π	0.369 828	0.369 846	0.243 144	0.227 048
7π	0.574 511	0.575 657	0.451 495	0.434 665
IVOs				
$5\pi'(5\pi^*)$	0.028 908	0.031 453	−0.101 577	−0.114 806
$6\pi'(6\pi^*)$	0.083 748	0.084 914	−0.056 134	−0.016 044
$7\pi'(7\pi^*)$	0.288 792	0.294 072	0.152 343	0.141 273
$\bar{\epsilon}_v$	−0.059 339	−0.056 562	−0.198 343	−0.205 628

[a] The two basis sets 4-31G and 6-31G* are used to study the isolated anion.

TABLE 2: Comparison of Low-Lying Excitation Energies (eV) for the Isolated Phenolate Anion as Computed with the First-, Second-, and Third-Order H^v Calculations Using 4-31G and 6-31G* Basis Sets

	4-31G			6-31G*		
states	H^v_{1st}	H^v_{2nd}	H^v_{3rd}	H^v_{1st}	H^v_{2nd}	H^v_{3rd}
IP[d]						
$1\ ^2A$	1.0456	0.7579	0.8777	1.1721	1.1610	1.1596
singlets						
$2\ ^1A$	4.6864	4.2021	4.3914	4.7624	4.1135	4.3821
$3\ ^1A$	6.1971	5.7995	5.6555	6.1929	5.7216	5.5564
$4\ ^1A$	7.5433	7.5349	7.1219	7.5834	7.4074	7.0009
$5\ ^1A$	7.8900	7.5082	7.3503	7.9464	7.3542	7.1892
$6\ ^1A$	8.6398	8.3631	8.0224	8.5895	8.1919	7.8831
$7\ ^1A$	9.0093	8.3313	8.2287	9.0688	8.1334	8.0936
triplets						
$1\ ^3A$	3.9832	3.4984	3.6882	3.9760	3.3816	3.6433
$2\ ^3A$	4.0867	4.1090	3.9326	4.1891	4.0711	3.9512
$3\ ^3A$	4.9535	5.4088	4.9477	4.9226	5.3247	4.8000
$4\ ^3A$	6.7536	7.1112	6.5252	6.6930	6.9518	6.2955
$5\ ^3A$	7.4497	7.6641	7.1912	7.5933	7.5988	7.1747
$6\ ^3A$	7.7047	7.4479	7.2691	7.6813	7.2110	7.1406
quintets						
$1\ ^5A$	8.6540	9.1280	8.5005	8.6344	8.9382	8.3213

[a] Ionization potential.

H^v_{3rd}/4-31G value), while the ionization potential increases by 0.2819 eV at third order. Thus the 6-31G* basis set does not offer a significant enough improvement over the 4-31G basis set to warrant the extra expense for larger model systems of PYP, where the H^v and many other high-level ab initio computations become prohibitive. A large basis set may be necessary for twisted geometries, when polarization contributions become important. Therefore, the following calculations all apply the 4-31G basis set.

To assess the accuracy of the H^v calculations, we perform a series EOM-CCSD, sa-CASSCF, sa-CASMP2, and CIS calculations for the isolated phenolate anion at the same ground-state optimized geometry obtained with the 4-31G basis. Table 3 presents the dominant configurations for the singlet and triplet excited states and their CI coefficients as calculated with various methods. These excited states have the same dominant configurations in the different calculations, which are compared below to each other.

Additionally, H^v calculations have also been made with smaller valence spaces involving five and six valence orbitals [i.e., 2π, 3π, 4π, $5\pi^*$, $6\pi^*$ (called 5V) and $7\pi^*$ (called 6V)] for the isolated phenolate anion. The 5V space performs better for the low-lying excitation energies at third-order than the 6V space as shown in Table 4. The H^v energies from the 5V and 7V spaces are quite close to each other in both second and third orders. Therefore, the 5V space provides a good approximation with reduced computational efforts, a feature that will be useful in extensions to the full PYP chromophore. However, we only discuss computations here obtained from the 7V space.

B. The Protein-Charged Models. The effective valence shell Hamiltonian (H^v) theory is now applied to study the electronic spectrum of a phenolate anion which is embedded in a positive (+1) point charge environment consisting of seven amino acids (Tyr 42, Glu 46, Thr 50, Arg 52, Cys 69, Phe 96, and Tyr 98). These amino acids form a closed amino acid shell as depicted in Figure 1. This model study serves to assess the quality of different approximations as a precursor to larger computations for the spectrum and photodynamics of the full protein bound chromophore of PYP.

The present calculations are based on the PYP structure which is determined at a 1.4 Å resolution by X-ray crystallography.[7] However, the hydrogen positions are not available from X-ray crystallography, and they must be generated using available information concerning the heavy atom coordinates. Thus, the hydrogen atom positions are generated here using eletronic structure computations and a two-step procedure: (i) First the individual geometries of the isolated amino acids and the anion are separately optimized for the hydrogen positions. These geometry optimizations are performed for Tyr 42, Glu 46, Thr 50 (charge = +1), Arg 52, the *para*-hydroxycinnamoyl anion covalently bound to Cys 69 via a thioester linkage, Phe 96 and Tyr 98 using restricted open shell Hartree−Fock (ROHF) computations with a 4-31G basis. Then (ii) the hydrogen-bond geometries are reoptimized for the supermolecular complex illustrated in Figure 3, where the positions of hydrogen atoms marked with asterisks are recomputed. The amino acid Phe 96 is excluded from the computation because a hydrogen bond cannot be formed between residue Phe 96 and its adjoining amino acids in PYP. The first step fixes the positions of all heavy atoms in the amino acids at their experimental geometries in the PYP, X-ray structure, while the calculations in the second step also allows optimization of certain bonds other than the hydrogen bonds. It is not surprising that the calculated structural parameters for those H atoms involved in H-bonds significantly differ in the two calculations, whereas the calculated hydrogen bond lengths and angles change only slightly for the remaining hydrogens not participating in H-bonds.

As a preliminary study to assess the quality of different approximations for treating PYP, the *para*-coumaric acid is replaced by a phenolate anion which represents an important portion of the PYP chromophore. To preserve as much of the local *para*-coumaric acid structure as possible, all structural parameters for the phenolate anion are maintained as identical to those of *para*-coumaric acid, except the single C′(1)−H′(1) bond length in Figure 4 is optimized for the isolated phenolate anion using RHF calculations and a 4-31G basis. Table 5 summarizes the optimized structure of the phenolate anion used for the calculations. The values employed for surrounding point charges to represent the seven adjacent and most strongly interacting amino acids emerge from the SCF calculations for the eight-acid supermolecular complex (*para*-coumaric acid, Tyr 42, Glu 46, Thr 50, Arg 52, Cys 69, Phe 96, and Try 98). Thus, this model treats the phenolate anion as the chromophore embedded in the charged protein environment. It is straight-

TABLE 3: Dominant Configuration(s) in the H^v, EOM-CCSD, sa-CASSCF, and CIS Wave Functions for the Low-Lying States of the Isolated Phenolate Anion

states	dominant configuration	H^v_{1st}	H^v_{2nd}	CI H^v_{3rd}	coefficient EOM-CCSD	sa-CASSCF[a]	CIS
singlets							
S_1	$4\pi \rightarrow 5\pi^*$	0.5942	0.6478	0.6279	0.6397	0.8699	0.6732
S_2	$4\pi \rightarrow 6\pi^*$	0.5759	0.6195	0.6134	0.6336	0.8180	0.6219
S_3	$2\pi \rightarrow 5\pi^*$	0.4094	0.4781	0.4200	0.4286	0.6544	
	$3\pi \rightarrow 6\pi^*$	0.3885	0.4255	0.4553	0.4872	−0.5125	
triplets							
T_1	$4\pi \rightarrow 5\pi^*$	0.6624	0.6805	0.6761	0.6749	0.9303	0.6883
T_2	$4\pi \rightarrow 6\pi^*$	0.6344	0.6714	0.6659	0.6549	0.9034	0.6066
T_3	$3\pi \rightarrow 5\pi^*$	0.6284	0.6696	0.6588	0.6493	0.8998	0.6061

[a] The sa-CASSCF calculations employ a complete active space with eight electrons occupying seven active orbitals. The state averages involve four low-lying states each for the singlets and triplets.

TABLE 4: Comparison of H^v $\pi \rightarrow \pi^*$ Excitation Energies (eV) for the Isolated Phenolate Anion with the 5V, 6V, and 7V Spaces Using a 4-31G Basis Set

	5V			6V			7V		
states	1st	2nd	3rd	1st	2nd	3rd	1st	2nd	3rd
triplets									
$4\pi \rightarrow 5\pi^*$	4.236	3.592	3.713	4.053	3.448	3.344	3.983	3.498	3.688
$4\pi \rightarrow 6\pi^*$	4.583	4.310	3.983	4.219	4.329	3.621	4.087	4.109	3.933
$3\pi \rightarrow 5\pi^*$	5.679	5.593	5.163	5.200	5.425	4.463	4.954	5.401	4.948
singlets									
$4\pi \rightarrow 5\pi^*$	5.552	4.015	4.661	4.956	4.096	4.176	4.686	4.202	4.391
$4\pi \rightarrow 6\pi^*$	6.899	5.255	6.093	6.555	5.052	6.003	6.197	5.799	5.656

forward to perform the H^v calculations for the phenolate anion in this point-charge field.

Clearly, the full chromophore in PYP is characterized by two important features that affect its electronic spectra: (1) the two hydrogen bonds with Tyr 42 and Glu 46 and (2) the thioester linkage. To clarity the influence of these two hydrogen bonds (with Tyr 42 and Glu 46) on the excitation energies for the phenolate anion in the charge field of surrounding amino acids, we also permit the phenolate anion to be hydrogen bonded to two water molecules which replace the Tyr 42 and Glu 46 amino acids. Table 5 also presents the molecule geometries for these two water molecules, where the two O−H bond lengths OH-HZ and OE2-HD in Figure 4 are determined by optimizations of these two bond lengths in SCF calculations for the phenolate anion−$2H_2O$ complex. Because the oxygen and hydrogen atoms OH and HH (or OE2 and HE2) in the Tyr 42 (or the Glu 46) are included in the water molecule, the corresponding point charges in the charge field are summed into charges for the atom CZ (or CD) in Tyr 42 (or Glu 46). The following demonstrates that these two hydrogen bonds do not significantly affect the excitation energies of the protein-bound phenolate anion. Moreover, as will be discussed elsewhere,[43] the presence of thioester linkage substantially decreases the vertical excitation energies to the low-lying states of the full chromophore (a decrease of about 1 eV for the lowest singlet excited state).

IV. Results and Discussions

Table 6 compares the H^v excitation energies for the isolated phenolate anion with those computed from the EOM-CCSD, sa-CASSCF, and sa-CASMP2 methods using the same basis set (4-31G). The comparison demonstrates that the second-order H^v_{2nd} excitation energies are in good agreement with the EOM-CCSD energies. Differences vary from just 0.2172 eV for the first singlet excited state to no more than 0.0387 eV for the next two higher singlet excited states. The difference between the H^v_{2nd} and H^v_{3rd} excitation energies for the first two singlet states S_1 ($4\pi \rightarrow 5\pi^*$) and S_2 ($4\pi \rightarrow 6\pi^*$) is only 0.167 eV on average, implying that the laborious third order corrections are not important for these two excited states. Thus, the second order H^v suffices to treat the singlet excited states for the isolated phenolate anion. Additionally, the sa-CASMP2 energies are higher than the corresponding sa-CASSCF values for all three singlet and triplet excited states of the phenolate anion. The CIS energies for the S_1 and S_2 states are 5.4755 and 6.4121 eV, which are much higher than the EOM-CCSD and H^v_{3rd} (or H^v_{2nd}) energies, thus reflecting the often poor performance of the widely used CIS approach. A rather low S_1 excitation energy has been obtained from a first-order configuration interaction calculation (FOCI) generated by including all single excitations from the CAS multireference base (see the 3.6043 eV entry in Table 6), where the ground and the lowest excited-state geometries are taken as those optimized with CASSCF calculations using a 6-31G basis set.[31] This again illustrates the strong limitations of FOCI method for excited states. Similarly, when the ground- and excited-state geometries are optimized at the CASSCF level, a low excitation energy (3.69 eV) is likewise obtained with the CASPT2 method.[32]

A peak in the photodetachment spectrum of the phenolate anion has been interpreted as due to the excitation of a quasibound excited state, a Fesbach resonance.[33] The peak in the experimental spectrum lies at roughly 330 nm, which translates into a vertical excitation energy of 3.76 eV, which is somewhat lower that our computed range of 4.2−4.4 eV. However, the accurate determination of the anion excitation energy requires the use of larger basis sets with diffuse functions, while the protein bound anion with a stabilizing background positive charge is adequately treated with the smaller basis sets employed. Our computations for the isolated anion are provided to compare the H^v calculations with other methods and to establish a vaible set of approximations for use in describing the protein bound system.

The H^v_{3rd} excitation energies for the three triplet states agree with the sa-CASMP2 energies to within 0.043 eV in Table 6, whereas these triplet state excitation energies also exhibit certain differences between the H^v_{2nd} and H^v_{3rd} calculations. The H^v_{2nd} thus yields a slightly poorer description for the triplet states

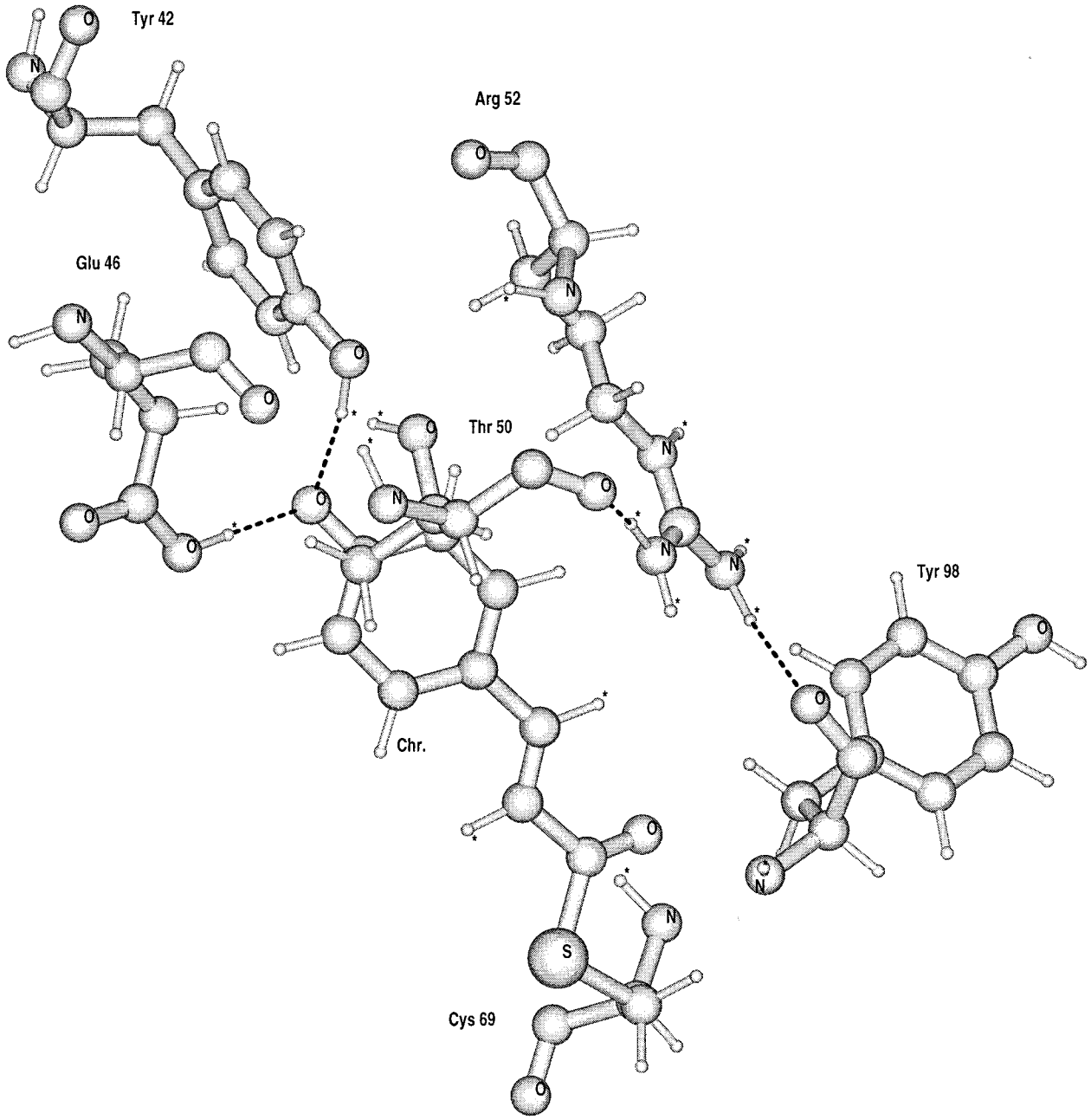

Figure 3. Large molecular complex used for optimization of the hydrogen bond geometries in PYP. The geometrical parameters for the hydrogen atoms marked by an asterisk are reoptimized for this molecular complex using ROHF calculations and a 4-31G basis, while other atoms are fixed at the experimental or previously calculated geometries. The dashed lines indicate the four strong intermolecular hydrogen bonds.

than for the singlet states. This difference has no influence on our study because, so far, no triplet excited states have been experimentally observed in the photocycle of the PYP.

Hydrogen Bonds. Hydrogen bonds are essential features of the PYP protein. The difference between the ground-state energy for the optimized hydrogen-bond geometry of the large complex and that for the sum of the ground-state energies of the isolated amino acids provides the binding energy ($-\Delta E$) for hydrogen bonding in the PYP chromophore. ROHF/4-31G computations yield $-\Delta E = 81.58$ kcal/mol as the total binding energy due to the seven hydrogen bonds which form the hydrogen bonded network in PYP.

Six intermolecular hydrogen bonds are easily identified in the optimized H-bond structure of Figure 3 by applying the criterion that intermolecular hydrogen bonds correspond to hydrogen-acceptor distances that are shorter than 2.4 Å and that the angle between the hydrogen, the atom to which the hydrogen is covalently bound, and the acceptor is smaller than 35°.[34] Table 7 summarizes the relevant hydrogen-bond structural parameters using the same atom labels as those in the PDB file (2PHY). Table 7 indicates and Figures 1 and 3 exhibit the presence of four strong intermolecular hydrogen bonds: the Tyr 42 and Glu 46 hydrogens are H-bonded with the chromophore's phenolic oxygen and the Arg 52 hydrogens are H-bonded with the carbonyl oxygen atoms of Thr 50 and Tyr 98. In addition, the Thr 50 hydrogen bonds with Try 42 and with the carbonyl oxygen of Glu 46. Moreover, the distance from the thioester oxygen to the hydrogen in Cys 69 is 2.2298 Å, while the angle between H−N(Cys 69)−O1(thioester oxygen) is 52.5462°. This reflects the presence of an intramolecular hydrogen bond between the thioester oxygen and the backbone amide of Cys 69. On average, each hydrogen bonding interaction in the hydrogen-bonded network yields a binding energy of approximately 11.65 kcal/mol, which is somewhat larger than the

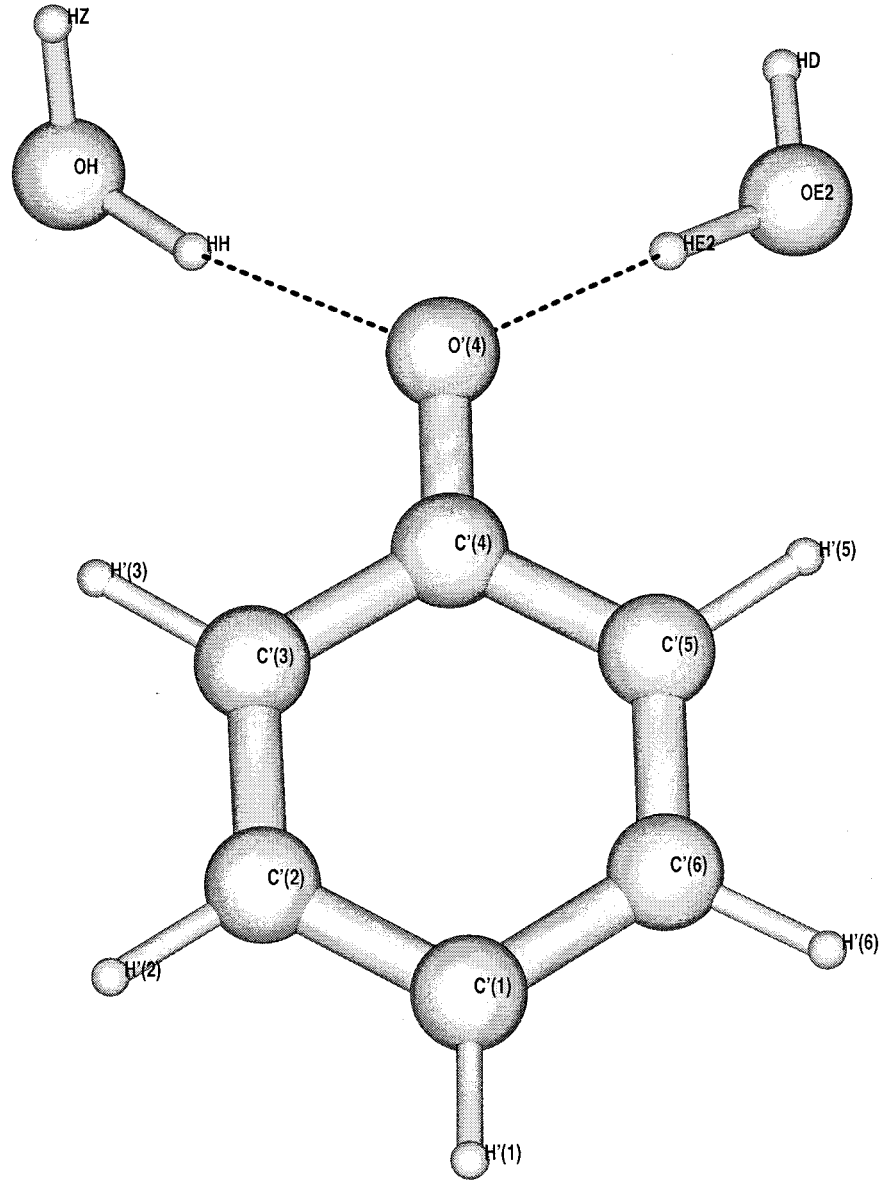

Figure 4. Structure of the phenolate anion with two hydrogen-bonded water molecules.

individual binding energy of 10.4 kcal/mol obtained from the computation for the phenol-H_2O complex.[35]

Charge Distributions. A thorough investigation of the PYP chromophore requires an analysis of the charge distributions for the chromophore and its surroundings. Figure 5 depicts the net partial atomic charges for the *para*-hydroxycinnamoyl anion covalently bonded to the amino acid Cys 69 via a thioester linkage. The partial charges are derived both by using a Mulliken population analysis[36] and by fitting to the electrostatic potential according to two alternative Merz−Singh−Kollman (MK)[37,38] and the CHelpG[39] schemes. The partial charge determinations are based on HF/4-31G calculations for the hydrogen-bonded supermolecular complex of Figure 3, with the amino acid Phe 96 also included. Obviously, the net negative charges are concentrated primarily on the phenolic oxygen and on the thioester oxygen. These negative charge concentrations favor the formation of the three hydrogen bonds (see Table 7 for definition of atom labels): O'_4(Chr.)...HH − OH(Tyr42), O'_4(Chr.)...HE2 − OE2(Glu46) and O1(thioester)...H−N(Cys69), where Chr. designates the chromophore. In contrast, the partial atomic charge distribution derived from semiempirical PM3 quantum-mechanical calculations (using MOPAC[40]) have the negative charge distributed over the whole system, without any particular concentration on the heavy atoms (see Figure 5). The semiempirical charge distribution, therefore, does not foster the formation of these hydrogen bonds. Moreover, all of our calculations of the atomic charges in PYP indicate that the net positive charge of the amino acid Arg 52 is concentrated on the carbon atom CZ, but not on the nitrogen NE, which means that the positive charge of Arg 52 lies rather far from the chromophore's phenolic oxygen. This supports a conclusion based on experimental observation that Arg 52 is not required for charge stablization of the chromophore.[41] In other words, Arg 52 interacts with Tyr 98, rather than with the chromophore.[42]

The total partial charges computed for each of the amino acids from the HF/4-31G calculation for the eight-acid complex are −0.0323(Mulliken), −0.0419(MK), 0.0386(CHelpG) for Tyr 42; −0.07691, −0.05811, −0.1060 for Glu 46; −0.01956, −0.1325, −0.07958 for Thr 50; 0.9195, 1.0326, 0.9592 for Arg 52; 0.1734, −0.0381, −0.1187 for Cys 69; 0.0006, −0.0280, −0.0175 for Phe 96; 0.0242, 0.1087, 0.1380 for Tyr 98; and −0.9890, −0.8427, −0.8142 for Chr. These charges indicate that small intermolecular charge transfers accompany the

TABLE 5: Combination of Experimental and Calculated Coordinates for the Phenolate Anion and for the Two Hydrogen-Bonded Waters in the Protein-Bound Model[a]

atoms	*X*	*Y*	*Z*
phenolate			
C′(1)	14.870	0.383	−18.885
C′(2)	15.720	−0.403	−19.660
C′(3)	16.777	−1.097	−19.080
C′(4)	16.983	−0.994	−17.723
C′(5)	16.155	−0.224	−16.933
C′(6)	15.106	0.456	−17.515
O′(4)	17.939	−1.579	−17.197
H′(1)	14.121	0.966	−19.390
H′(2)	15.547	−0.474	−20.720
H′(3)	17.443	−1.705	−19.654
H′(5)	16.354	−0.174	−15.884
H′(6)	14.470	1.051	−16.888
$2H_2O$			
OH (Tyr42)	19.120	−3.709	−18.386
HH	18.664	−2.897	−18.064
HZ	20.055	−3.666	−18.229
OE2 (Glu46)	17.706	−2.175	−14.588
HE2	17.832	−1.915	−15.537
HD	18.255	−2.838	−14.200

[a] The coordinates for the heavy atoms are taken from the X-ray data, 2PHY, in the Protein Data Bank, while the coordinates for the H atoms are calculated using ROHF calculations with a 4-31G basis. The coordinates are in angstroms. The residue labels for the water molecules represent the amino acids whose H bonds are replaced by the H_2O hydrogen bonds.

hydrogen bonding, with a range of approximately 0.02−0.20 electrons transferred between these amino acids and the chromophore. Of course, the ground state behavior may not adequately describe the alterations of the partial charges in the (veritcal) excited states where high level correlated ab initio computations are not possible for the full supermolecular complex. Nevertheless, the small charge transfers from or to the chromophore support the use of a model involving a phenolate anion surrounded by the seven charged amino acids as an initial model system for studying excitation energies of the PYP chromophore.

The Phenolate Anion in the Environment of PYP. We have performed a series of H^v calculations for the two simplified models of the chromophore in PYP mentioned above, namely, the protein-bound phenolate anion and the phenolate anion−$2H_2O$ complex in the PYP−protein environment. The protein environment is simply described as a background charge distribution that has been obtained via the three procedures: Mulliken, MK, and CHelpG populations, of which the Mulliken population is easily obtained from the SCF molecular orbital formalism. To examine how the three different sets of atomic charge populations affect the computed excitation energies for the chromophore, H^v and CAS calculations have been performed for the protein-bound phenolate anion in the field of the Mulliken, MK, and CHelpG charge distributions. The computational steps proceed in an identical manner as those for the isolated phenolate anion. The results are summarized in Table 8. The three charge distributions provide very similar sets of singlet and triplet excitation energies of the protein-bound phenolate anion for all calculations considered. Particularly, the differences in the excitation energies to the first singlet excited state (S_1), the primary excitation energy of interest, with the Mulliken, MK and CHelpG charge distributions are just within 0.089 eV. However, only the Mulliken charges stabilize the S_1 state H^v excitation energies below the lowest ionization potental, which varies more (0.68 eV) with the charge distribution. The maximum difference in the energies of Table 8 is 0.2085 eV, which emerges for the second singlet state excitation energy with the sa-CASSCF calculation. Table 8 shows that the Mulliken analysis provides the lowest set of excitation energies to the three singlet and triplet excited states (except for the T_2 first-order H^v energy). For the latter reasons and because of the minor differences between the three sets of charges and because the main trends of interest here are similarly unchanged by the choice among the different charge sets, the Mulliken populations are used in all following calculations.

As noted above the H^v calculations can be performed for the phenolate anion−$2H_2O$ complex in the PYP environment. The H^v orbital energies are also summarized in Table 1 for the two protein models. The (4-31G basis set) valence orbital energies in Table 1 gradually decrease as the environment becomes more stabilizing to the phenolate ion upon first adding the point-charge field and then upon appending the two water molecules. This general decrease is in line with expections that the positively charged PYP protein environment stabilizes both the ground and excited states of the chromophore.

Table 9 compares the low-lying excitation energies for the isolated phenolate anion and for the two PYP models as computed with first-, second-, and third-order ab initio H^v calculations, as well as with the sa-CASSCF (or CASSCF), sa-CASMP2 (or CASMP2) and CIS methods. The dominant configurations for the electronic states are compared in Table 10 for the calculations by the different approaches. In these three systems, the sa-CASSCF energies almost reproduce the CASSCF energies for the first singlet state, while for the lowest triplet state they are slightly higher than the CASSCF values. This indicates that the sa-CASSCF method should provide reliable results at least for the lowest singlet excited state, a finding that will be useful in computations for the whole chromophore. A striking feature in Table 9 is that the lowest excitation energies for both the singlet and triplet states (S_1 and T_1) increase by 0.1269 and 0.1651 eV (the average shift from the sa-CASSCF, CASSCF and sa-CASMP2, CASMP2 calculations) for the

TABLE 6: Comparison of H^v $\pi \rightarrow \pi^*$ Excitation Energies (eV) for the Isolated Phenolate Anion with Calculations Using the EOM-CCSD, sa-CASSCF, sa-CASMP2, and CIS Methods; All Computations Use a 4-31G Basis Set[a]

states	H^v_{1st}	H^v_{2nd}	H^v_{3rd}	EOM-CCSD	sa-CASSCF	sa-CASMP2	CIS	FOCI[b]
singlets								
S_1: $4\pi \rightarrow 5\pi^*$	4.6864	4.2021	4.3914	4.4193	4.2881	4.3951	5.4755	3.6043
S_2: $4\pi \rightarrow 6\pi^*$	6.1971	5.7995	5.6555	5.7608	6.0372	6.1112	6.4121	
S_3: $2\pi \rightarrow 5\pi^*$	7.5433	7.5349	7.1219	7.4965	7.3032	7.4281		
$3\pi \rightarrow 6\pi^*$								
triplets								
T_1: $4\pi \rightarrow 5\pi^*$	3.9832	3.4984	3.6882	3.6106	3.5797	3.6919	3.6712	3.3363
T_2: $4\pi \rightarrow 6\pi^*$	4.0867	4.1090	3.9326	3.8712	3.8295	3.9454	3.7650	4.4338
T_3: $3\pi \rightarrow 5\pi^*$	4.9535	5.4088	4.9477	5.0024	4.8942	4.9904	4.6463	

[a] The EOM-CCSD calculations use the ACES II program, while the sa-CASMP2 and CIS calculations are performed with the *Gaussian 98* (G98 Revision A.6) program package. [b] Using the CAS-MSCF optimized geometries with a 6-31G basis from ref 31.

TABLE 7: The Calculated Hydrogen-Bond Geometry Parameters for PYP[a]

	$d_{O\cdots H}$ (Å)		∠HO(or N)O
O'_4(Chr.)...HH(Tyr42)	1.7362	∠HH−OH(Tyr42)...O4′(Chr.)	6.9870°
O'_4(Chr.)...HE2(Glu46)	1.6969	∠HE2−OE2(Glu46)...O4′(Chr.)	3.3582°
O(Thr50)...1HH1(Arg52)	2.0065	∠1HH1−NH1(Arg52)...O(Thr50)	13.6311°
O(Tyr98)...2HH2(Arg52)	1.9348	∠2HH2−NH2(Arg52)...O(Tyr98)	6.5082°
OH(Tyr42)...HG1(Thr50)	2.0436	∠HG1−OG1(Thr50)...O(Tyr42)	28.2623°
O(Glu46)...H(Thr50)	2.1389	∠H−N(Thr50)...O(Glu46)	28.2646°

[a] The atom labels are taken as those in the 2PHY file of the Protein Data Bank (the PDB web page is http://www.pdb.bnl.gov).

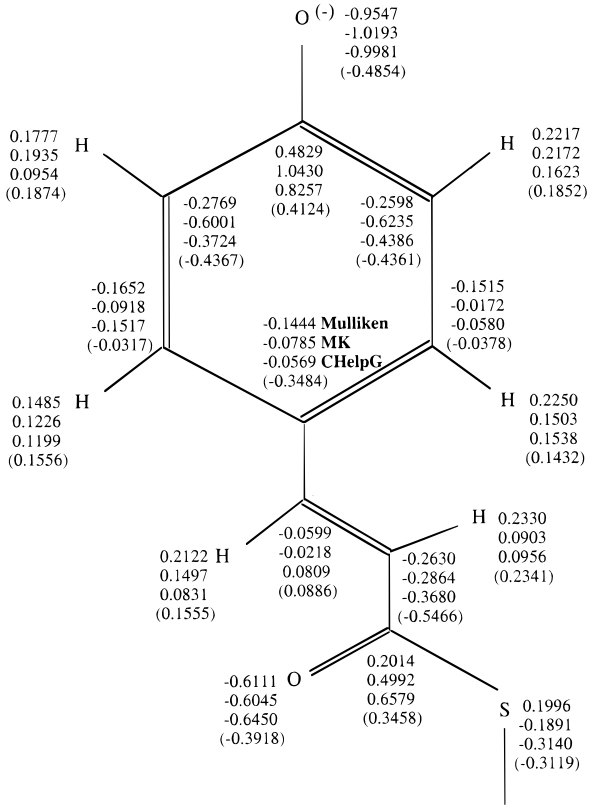

Figure 5. Atomic partial charges on the chromophore as computed with the ROHF calculations for the large molecular complex (see the text) using a 4-31G basis. The values in parentheses are computed semiempirically with the PM3 Hamiltonian of MOPAC.

protein-bound phenolate anion with the two water molecules as compared to the protein-bound phenolate anion. This suggests that the two hydrogen bonds stabilize the ground state of the PYP chromophore more than the first singlet excited state. The higher excited states behave in a like manner, and a similar trend emerges also for the H^{v}_{1st} and H^{v}_{3rd} calculations but not for all the H^{v}_{2nd} values (see Table 9). The two hydrogen bonds in the protein-bound anion$-2H_2O$ complex contributes 0.3172 eV to the lowest singlet excitation energy and 0.2014 eV to the lowest triplet excitation energy in the H^{v} calculations (using an absolute average of the H^{v}_{1st}, H^{v}_{2nd}, and H^{v}_{3rd} values). Hence, the two hydrogen bonds likewise do not affect the lower excited states significantly. Table 9 also exhibits large gaps (>1 eV) between the S_1 and S_2 excited states for the three different models. As expected, a $n \rightarrow \pi^*$ excited state is also present between the first and second singlet excited $\pi \rightarrow \pi^*$ states, as will be described in a further work.[43]

The positively charged field of the amino acid environment clearly stabilizes the negatively charged phenolate anion. The RHF ground-state energy of the protein-bound phenolate anion is −315.125328 hartree, which is much lower than the energy (−304.531122 hartree) of the isolated anion (see Table 1). However, Table 9 displays an increase in the calculated H^{v} excitation energies by only 0.22 eV (0.33 eV) on average for the H^{v}_{1st}, H^{v}_{2nd}, and H^{v}_{3rd} excitation energies to the lowest singlet (triplet) excited state in passing from the isolated system to the protein-bound phenolate anion. Likewise, the (sa-)CASSCF and (sa-)CASMP2 calculations yield the lowest excited singlet (or triplet) excitation energy for the protein-bound anion as about 0.31 eV (or 0.46 eV) higher than for the isolated phenolate anion. The comparisons indicate that the H^{v}_{2nd} calculations usually provide lower energies than the H^{v}_{3rd} and (sa-)CASMP2 treatments, Despite the large overestimate of singlet excitation energies by the CIS method, the ordering of the CIS singlets matches the H^{v} calculations (see Table 9). Finally, we note that the excitation energies for the protein-

TABLE 8: Effect of the Atomic Charges, Derived via Different Procedures, on the Low-Lying Excitation Energies and the Ionization Potential IP (eV) from H^{v} (or CAS) Calculations for the Protein-Bound Phenolate Anion Using the 4-31G Basis Set

states	Mulliken	MK	ChelpG
singlets			
S_1: $4\pi \rightarrow 5\pi^*$			
H^{v}_{1st}	4.8671	4.8850	4.8998
H^{v}_{2nd}	4.4686	4.5111	4.5570
H^{v}_{3rd}	4.5904	4.6145	4.6404
sa-CASSCF	4.6033	4.6391	4.6693
CASSCF	4.6491	4.6989	4.7378
CASMP2	4.8967	4.9290	4.9307
S_2: $4\pi \rightarrow 6\pi^*$			
H^{v}_{1st}	6.6790	6.7815	6.8650
H^{v}_{2nd}	6.0971	6.1682	6.2193
H^{v}_{3rd}	6.0580	6.1318	6.1919
sa-CASSCF	6.4741	6.5910	6.6826
S_3: $2\pi \rightarrow 5\pi^*$			
$3\pi \rightarrow 6\pi^*$			
H^{v}_{1st}	7.7300	7.7566	7.7835
H^{v}_{2nd}	7.5781	7.5969	7.6145
H^{v}_{3rd}	7.2601	7.2914	7.3140
sa-CASSCF	7.4948	7.5296	7.5597
triplets			
T_1: $4\pi \rightarrow 5\pi^*$			
H^{v}_{1st}	4.4014	4.4360	4.4688
H^{v}_{2nd}	3.7940	3.8401	3.8963
H^{v}_{3rd}	3.9696	3.9929	4.0348
T_2: $4\pi \rightarrow 6\pi^*$			
H^{v}_{1st}	4.1938	4.1864	4.1855
H^{v}_{2nd}	4.4712	4.5133	4.5345
H^{v}_{3rd}	4.2214	4.2394	4.2440
T_3: $3\pi \rightarrow 5\pi^*$			
$4\pi \rightarrow 6\pi^*$			
H^{v}_{1st}	4.9666	4.9964	5.0132
H^{v}_{2nd}	5.2647	5.2714	5.2722
H^{v}_{3rd}	4.8505	4.8680	4.8760
IP			
H^{v}_{1st}	5.1541	4.5052	4.7071
H^{v}_{2nd}	4.6302	3.9581	4.1390
H^{v}_{3rd}	4.9449	4.2664	4.4507

TABLE 9: Comparison of Low-Lying Excitation Energies (eV) from Various Calculations for the Isolated, Protein-Bound Phenolate Anion and the Protein-Bound Phenolate Anion−2H$_2$O Complex Using the 4-31G Basis Set

states	isolated anion	bound anion	bound anion−2H$_2$O complex
singlets			
S$_1$: $4\pi \rightarrow 5\pi^*$			
H^v_{1st}	4.6864	4.8671	5.1666
H^v_{2nd}	4.2021	4.4686	4.2605
H^v_{3rd}	4.3914	4.5904	5.1345
sa-CASSCF	4.2881	4.6033	4.7252
sa-CASMP2	4.3951	4.7158	4.8428
CASSCF	4.2833	4.6491	4.8028
CASMP2	4.6514	4.8967	5.0015
CIS	5.4755	5.6883	5.8141
S$_2$: $4\pi \rightarrow 6\pi^*$			
H^v_{1st}	6.1971	6.6790	7.0303
H^v_{2nd}	5.7995	6.0971	5.7083
H^v_{3rd}	5.6555	6.0580	6.3875
sa-CASSCF	6.0372	6.4741	6.6889
sa-CASMP2	6.1112	6.5481	6.7630
CIS	6.4121	6.6024	6.5885
S$_3$: $2\pi \rightarrow 5\pi^*$			
$3\pi \rightarrow 6\pi^*$			
H^v_{1st}	7.5433	7.7300	8.2172
H^v_{2nd}	7.5349	7.5781	7.3768
H^v_{3rd}	7.1219	7.2601	7.4478
sa-CASSCF	7.3032	7.4948	7.5959
sa-CASMP2	7.4281	7.6209	7.7294
triplets			
T$_1$: $4\pi \rightarrow 5\pi^*$			
H^v_{1st}	3.9832	4.4014	4.6405
H^v_{2nd}	3.4984	3.7940	3.6758
H^v_{3rd}	3.6882	3.9696	4.2166
sa-CASSCF	3.5797	4.1749	4.3414
sa-CASMP2	3.6919	4.2844	4.4436
CASSCF	3.4897	3.9131	4.0835
CASMP2	3.8015	4.0486	4.2129
CIS	3.6712	4.0242	4.1659
T$_2$: $4\pi \rightarrow 6\pi^*$			$3\pi \rightarrow 5\pi^*$
H^v_{1st}	4.0867	4.1938	4.3358
H^v_{2nd}	4.1090	4.4712	4.5214
H^v_{3rd}	3.9326	4.2214	4.3591
sa-CASSCF	3.8295	3.9771	4.0041
sa-CASMP2	3.9454	4.0918	4.1201
CIS	3.7650	3.7871	3.7689
T$_3$: $3\pi \rightarrow 5\pi^*$		$4\pi \rightarrow 6\pi^*$	
H^v_{1st}	4.9535	4.9666	5.1120
H^v_{2nd}	5.4088	5.2647	5.1699
H^v_{3rd}	4.9477	4.8505	4.8191
sa-CASSCF	4.8942	4.8426	4.8921
sa-CASMP2	4.9904	4.9341	4.9808
CIS	4.6463	4.7938	4.8893

bound phenolate anion (with and without the two water molecules) are somewhat higher than those for the isolated system. However, these increases in excitation energies are insufficient to determine whether the lowest singlet excited state is unstable (i.e., a quasibound state) in the positively charged field of the surroundings. On the contrary, as we now discuss, the net positively charged protein field dramatically leads, as expected, to an increase in the vertical ionization potential as exhibited in Table 11. Thus the first singlet excited-state becomes stablized below the lowest ionization potential of the protein-bound phenolate anion.

The H^v calculations yield, with no additional effort, the vertical ionization potentials (IP) which are presented in Table 11 for the phenolate anion using the three models, along with (sa-)CASSCF, (sa-)CASMP2, and ROHF-MPn ($n = 2, 3, 4$)[44−47]

TABLE 10: Comparison of Dominant Configurations from the H^v, sa-CASSCF, and CIS Wave Functions for the Excited Singlet and Triplet States of the Protein-Bound Phenolate Anion and Phenolate Anion−2H$_2$O Complex

states	dominant configuration	H^v_{1st}	CI coefficient H^v_{2nd}	H^v_{3rd}	sa-CASSCF	CIS
			Bound Anion			
singlets						
S$_1$	$4\pi \rightarrow 5\pi^*$	0.5794	0.6475	0.6194	0.8254	0.6654
S$_2$	$4\pi \rightarrow 6\pi^*$	0.5339	0.5889	0.5748	0.8140	0.5775
S$_3$	$2\pi \rightarrow 5\pi^*$	0.3645	0.2904	0.3491	−0.4792	
	$3\pi \rightarrow 6\pi^*$	0.3331	0.3447	0.4264	0.5187	
triplets						
T$_1$	$4\pi \rightarrow 5\pi^*$	0.5274	0.6790	0.6414	0.7183	0.5915
T$_2$	$4\pi \rightarrow 6\pi^*$	0.4218	0.6489	0.5791	0.5862	0.4021
T$_3$	$3\pi \rightarrow 5\pi^*$	0.5326	0.6636	0.6181	0.7793	0.4921
	$4\pi \rightarrow 6\pi^*$	0.3761		0.2531	−0.5079	−0.4984
			Anion−2H$_2$O			
singlets						
S$_1$	$4\pi \rightarrow 5\pi^*$	0.5782	0.6435	0.6143	0.8017	0.6578
S$_2$	$4\pi \rightarrow 6\pi^*$	0.5467	0.6054	0.5408	0.8183	0.5745
S$_3$	$2\pi \rightarrow 5\pi^*$	−0.3257	−0.3668	−0.2453	−0.4632	
	$3\pi \rightarrow 6\pi^*$	0.3749	0.4296	0.5143	0.5149	
triplets						
T$_1$	$4\pi \rightarrow 5\pi^*$	0.6241	0.6725	0.4909	0.8859	0.6651
T$_2$	$4\pi \rightarrow 6\pi^*$	0.5003	0.6257	0.4820	0.6926	0.4426
	$3\pi \rightarrow 5\pi^*$	−0.3808	−0.2204		0.5504	0.4566
T$_3$	$3\pi \rightarrow 5\pi^*$	0.5297	0.6351	0.6566	0.7326	0.4814
	$4\pi \rightarrow 6\pi^*$	0.3976	0.2041	0.1762	−0.5691	−0.5087

TABLE 11: Comparison of the Ionization Potential (eV) from the First-, Second-, and Third-Order H^v Calculations with (sa-)CASSCF, (sa-)CASMP2, and ROHF-MPn Calculations ($n = 2, 3, 4$) for the Isolated, Protein-Bound Phenolate Anion, and the Protein-Bound Phenolate Anion−2H$_2$O Complex Using the 4-31G Basis Set[a]

methods	isolated anion	bound anion	bound anion−2H$_2$O complex
H^v_{1st}	1.0456	5.1541	5.9649
H^v_{2nd}	0.7579	4.6302	4.6180
H^v_{3rd}	0.8777	4.9449	5.8824
sa-CASSCF	−0.0963	4.0629	4.5541
sa-CASMP2	0.6894	4.8058	5.3192
CASSCF	0.0579	4.1839	4.6724
CASMP2	1.0779	5.0591	5.5735
MP2	1.4811	5.1468	5.5305
MP3	1.2059	5.0350	5.4282
MP4	1.3241	5.0388	5.4294

[a] The (sa-)CASMP2 and ROHF-MPn calculations ($n = 2, 3, 4$) are performed with the *Gaussian 98* program (G98 Revision A.6).

IPs. All the calculations display the phenolate anion IP as substantially increasing by about 4 eV in passing from the isolated anion to the protein-bound anion, and then further increasing by 0.4−0.9 eV for the protein-bound anion−2H$_2$O complex. (The H^v_{2nd} calculations have the latter two IPs almost the same.) This behavior clearly arises because the phenolate anion lies in the chromophore-binding pocket. The substantial increase in the IP for the protein-bound anion implies that the S$_1$ state is bound in PYP. Thus, our calculations demonstrate that the electrostatic enviroment of PYP stablizes the lowest singlet excited state from a quasibound resonance in the isolated phenolate anion, whereas the two H-bonds have a minor influence on any stabilization. Additionally, some differences of the H^v IPs from the other calculations emerge partially because the energy of the radical state is obtained in the H^v method as a byproduct of the anion computation and not from a separate treatment of the radical as in the MPn (or CASMP2) case. The H^v_{3rd}, CASMP2 and MP4 IPs are fairly comparable to each other for the protein-bound model, but significant

TABLE 12: Comparison of IPs and Low-Lying Singlet Excitation Energies (eV) from (sa-)CASSCF and (sa-)CASMP2 Calculations for the Isolated, Protein-Bound Phenolate Anion and the Protein-Bound Phenolate Anion−2H_2O Complex Using the 4-31G and 6-311G Basis Sets[a]**

states	isolated anion 4-31G	6-311G**	bound anion 4-31G	6-311G**	anion −2H_2O 4-31G	6-311G**
IP						
sa-CASSCF	−0.0963	0.1895	4.0629	4.2998	4.5541	4.6165
sa-CASMP2	0.6894	1.6035	4.8058	5.5957	5.3192	5.9254
CASSCF	0.0579	0.3763	4.1839	4.4332	4.6724	4.7479
CASMP2	1.0779	2.1186	5.0591	5.8752	5.5735	6.2146
absolute diff.[a]						
CASSCF	0.3021		0.2431		0.0690	
CASMP2	0.9774		0.8030		0.6237	
singlets						
$4\pi \rightarrow 5\pi^*$						
sa-CASSCF	4.2881	4.2886	4.6033	4.5990	4.7252	4.6567
sa-CASMP2	4.3951	4.4029	4.7158	4.7360	4.8428	4.7988
CASSCF	4.2833	4.3014	4.6491	4.6518	4.8028	4.7305
CASMP2	4.6514	4.7727	4.8967	4.8832	5.0015	4.9151
$4\pi \rightarrow 6\pi^*$						
sa-CASSCF	6.0372	5.9603	6.4741	6.3704	6.6889	6.4877
sa-CASMP2	6.1112	6.0456	6.5481	6.4241	6.7630	6.5189
$2\pi \rightarrow 5\pi^*$						
$3\pi \rightarrow 6\pi^*$						
sa-CASSCF	7.3032	7.2368	7.4948	7.4206	7.5959	7.4623
sa-CASMP2	7.4281	7.4209	7.6209	7.6049	7.7294	7.6444
absolute diff.[a]						
CASSCF	0.0405		0.0462		0.1149	
CASMP2	0.0505		0.0434		0.1169	

[a] The average absolute differences between the two basis sets including CASSCF (or CASMP2) and sa-CASSCF (or sa-CASMP2) calculations.

differences appear, as expected, for the isolated anion where the IP corresponds to the isolated anion electron affinity which, as is well-known, is quite difficult to compute and probably requires the use of diffuse functions for the negative ion. The stabilizing influence of the positively charged protein environment renders the IP computations for the protein bound system as those typical for "normal" neutral system IPs where both H^v and MP4 should be accurate.

To examine the presence of possible deficiencies in the basis set, we have performed additional (sa-)CASSCF and (sa-)CASMP2 calculations with the larger 6-311G** basis set for the three models. The results summarized in Table 12 indicate that as expected, shifts induced for the isolated and protein-bound cases by the polarization functions and the expansion of the basis set to triple-ζ are within 0.1 eV (on average 0.05 eV) for the (sa-)CASSCF and (sa-)CASMP2 calculations of the singlet excited states. The largest difference between the two basis sets appears for the CASMP2 IP of the problematic isolated anion, where the shift is 1.0407 eV. Nevertheless, the basis set differences for the singlet states of the protein-bound phenolate anion−2H_2O complex are still rather small (on average not more than 0.12 eV). Consequently, the 4-31G basis set provides a reasonable description of the phenolate anion electronic structure in the protein-bound environment. Of course it is possible that other basis sets, for example, an atomic natural orbital (ANO) basis set,[48,49] may give somewhat more accurate results, but we stick with the smaller basis since that is the most feasible for treating the full protein bound chromophore system.

V. Conclusions

We have performed a series of H^v calculations for the phenolate anion and have compared them to several EOM-CCSD, (sa-)CASSCF, (sa-)CASMP2, and CIS calculations. Although the interations between the different molecules in the PYP system are generally not negligible, the effects of the electrostatic environment of the PYP protein always predominate. Therefore, the present study mainly focuses attention on the influence of PYP electrostatic environment on the vertical excitation energies to the low-lying states of the chromophore. The influence of the electrostatic environment of the PYP protein is simulated by placing point charges to represent the electrostatic field of the seven amino acids near *para*-coumaric acid, the chromophore of PYP. Here we consider a phenolate anion in the field of these charges as the first simple model for the PYP chromophore to assess accurate approaches for treating the full protein-bound chromophore. The presence of hydrogen bonds between the oxygen of the phenolate anion and the Tyr 42 and Glu 46 residues is replaced, for simplicity, by hydrogen bonds between the oxygen of the phenolate anion and two water molecules.

An analysis of our calculations leads to the following general conclusions: (1) The *large* valence space H^v_{2nd} calculations (with 1225 reference configurations) accord well with most of the EOM-CCSD and sa-CASMP2 vertical excitation energies to low-lying excited singlet states of the phenolate anion in different environments. The H^v_{2nd} calculations are of comparable accuracy but are much easer and of much lower computational cost to implement than either MRCCSD, EOM-CCSD, or sa-CASMP2 methods. Therefore, the H^v_{2nd} method provides a very attractive approach for calculating excitation energies of the full chromophore. (2) The electrostatic enviroment of PYP is essential in stablizing the lowest singlet excited state of the chromophore to lie below the first IP of the system, while the two hydrogen bonds of the chromophore with Tyr 42 and Glu 46 in PYP exert a minor influence on the lower excited states for the phenolate anion in the PYP environment. Different methods for assigning partial charges on the surrounding residues lead to rather minor changes in the lowest vertical excitation energies.

Both conclusions provide important insights that enable us to perform further CAS and H^v calculations for the full photoactive chromophore of PYP, namely, the protein bound *para*-coumaric acid [$(O^-)-(C_6H_4)-(CH)=(CH)-(CO)-$]. The present work indicates that it will suffice in this future study to

apply the CAS and H^{v}_{2nd} methods to the excited-state potential energy surfaces of *para*-coumaric acid in the environment of PYP as a function of twisting about the double bond −(CH)═(CH)−. This type of information is probably vital for understanding the photodynamics of PYP.

Acknowledgment. This research is supported, in part, by NSF Grant CHE 9727655 and by UC/Argonne Grant 96-006. We thank Keith Moffat and Paul Bash for helpful discussions.

References and Notes

(1) Meyer, T. E. *Biochim. Biophys. Acta* **1985**, *806*, 175.
(2) Meyer; T. E.; Yakali, E.; Cusanovich, M. A.; Tollin, G. *Biochemistry* **1987**, *26*, 418.
(3) Hoff, W. D.; Kwa, S. L. S.; Van Grondelle, R.; Hellingwerf, K. J. *Phochem. Photobiol.* **1992**, *56*, 529.
(4) Hoff, W. D.; Van Stokkum, I. H. M.; Van Ramesdonk, H. J.; Van Brederode, M. E.; Brouwer, A. M.; Fitch, J. C.; Meyer, T. E.; Van Grondelle, R.; Hellingwerf, K. J. *Biophys. J.* **1994**, *67*, 1691.
(5) Imamoto, Y.; Kataoka, M.; Tokunaga, F. *Biochemistry* **1996**, *35*, 14047.
(6) Kort, R.; Vonk, H.; Xu, X.; Hoff, W. D.; Crielaard, W.; Hellingwerf, K. J. *FEBS Lett.* **1996**, *382*, 73.
(7) Borgstahl, G. E. O.; Williams, D. R.; Getzoff, E. D. *Biochemistry* **1995**, *34*, 6278.
(8) Perman, B.; Šrajer, V.; Ren, Z.; Teng, T. Y.; Pradervand, C.; Ursby, T.; Bourgeois, D.; Schotle, F.; Wulff, M.; Kort, R.; Hellingwerf, K.; Moffat, K. *Science* **1998**, *279*, 1946.
(9) Genick, U. K.; Soltis, S. M.; Kuhn, P.; Canestrelli, I. L.; Getzoff, E. D. *Nature* **1998**, *392*, 206.
(10) Iwata, S.; Freed, K. F. *J. Chem. Phys.* **1976**, *65*, 1071.
(11) Iwata, S.; Freed, K. F. *J. Chem. Phys.* **1977**, *66*, 1765.
(12) Sheppard, M. G.; Freed, K. F. *J. Chem. Phys.* **1981**, *75*, 4507.
(13) Sheppard, K. F. Freed, K. F. *J. Chem. Phys.* **1981**, *75*, 4525.
(14) Freed, K. F.; Sheppard, M. G. *J. Phys. Chem.* **1982**, *86*, 2130.
(15) Sekino, H.; Bartlett, R. J. *Int. J. Quantum Chem. Symp.* **1984**, *18*, 255.
(16) Greertsen, J.; Rittby, M.; Bartlett, R. J. *Chem. Phys. Lett.* **1989**, *164*, 57.
(17) Stanton, J. F.; Bartlett, R. J. *J. Chem. Phys.* **1993**, *98*, 7029.
(18) Roos, B. O. *Adv. Chem. Phys.* **1987**, *69*, 399.
(19) Andersson, K.; Malmqvist, P.-A.; Roos, B. O. *J. Chem. Phys.* **1992**, *96*, 1218.
(20) Frisch, M. J.; Trucks, G. W.; Schlegel, H. B.; Scuseria, G. E.; Robb, M. A.; Cheeseman, J. R.; Zakrzewski, V. G.; Montgomery, J. A., Jr.; Stratmann, R. E.; Burant, J. C.; Dapprich, S.; Millam, J. M.; Daniels, A. D.; Kudin, K. N.; Strain, M. C.; Farkas, O.; Tomasi, J.; Barone, M. Cossi, V.; Cammi, R.; Mennucci, B.; Pomelli, C.; Adamo, C.; Clifford, S.; Ochterski, J.; Petersson, G. A.; Ayala, P. Y.; Cui, Q.; Morokuma, K.; Malick, D. K.; Rabuck, A. D.; Raghavachari, K.; Foresman, J. B.; Cioslowski, J.; Ortiz, J. V.; Stefanov, B. B.; Liu, G.; Liashenko, A.; Piskorz, P.; Komaromi, I.; Gomperts, R.; Martin, R. L.; Fox, D. J.; Keith, T.; Al-Laham, M. A.; Peng, C. Y.; Nanayakkara, A.; Gonzalez, C.; Challacombe, M.; Gill, P. M. W.; Johnson, B.; Chen, W.; Wong, M. W.; Andres, J. L.; Gonzalez, C.; Head-Gordon, M.; Replogle, E. S.; Pople, J. A. *Gaussian 98*; Carnegie-Mellon University: Pittsburgh, PA, 1998.
(21) Herzenberg, A.; Sherrington, D.; Suveges, M. *Proc. Phys. Soc. London* **1964**, *84*, 465.
(22) Dunning, T. H.; McKoy, V. *J. Chem. Phys.* **1967**, *47*, 1735.
(23) Del Bene, J.; Pople, J. A. *J. Chem. Phys.* **2236**, *55*, 2236.
(24) Foresman, J. B.; Head-Gorden, M.; Pople, J. A.; Frisch, M. J. *J. Phys. Chem.* **1992**, *96*, 135.
(25) Finley, J. P.; Freed, K. F. *J. Chem. Phys.* **1995**, *102*, 102. Finley, J. P.; Chaudhuri, R. K.; Freed, K. F. *Phys. Rev. A* **1996**, *54*, 343.
(26) Kucharski, S. A.; Bartlett, R. J. *J. Chem. Phys.* **1991**, *95*, 8227.
(27) Finley, J. P. *J. Chem. Phys.* **1998**, *108*, 1081.
(28) Chaudhuri, R. K.; Finley, J. P.; Freed, K. F. *J. Chem. Phys.* **1997**, *106*, 4067.
(29) Sun, H.; Freed, K. F. *J. Chem. Phys.* **1982**, *76*, 5051.
(30) Nwobi, O.; Higgins, J.; Zhou, X.; Liu, R. *Chem. Phys. Lett.* **1997**, *273*, 155.
(31) Krauss, M.; Jensen, J. O.; Hameka, H. F. *J. Phys. Chem.* **1994**, *98*, 9955.
(32) Gao, J.; Li, N.; Freindorf, M. *J. Am. Chem. Soc.* **1996**, *118*, 4912.
(33) Richardson, J. H.; Stephenson, L. M.; Brauman, J. I. *J. Chem. Phys.* **1975**, *62*, 1580. The maximum wavelength in the photodetachment cross section in Figure 1 lies at about 330 nm (3.76 eV).
(34) Billeter, M.; Schaumann, T.; Braun, W.; Wüthrich, K. *Biopolymers* **1990**, *29*, 695.
(35) Schütz, M.; Burgi, T.; Leutwyler, S. *J. Mol. Struct.* (*Theochem*) **1992**, *276*, 117.
(36) Mulliken, R. S. *J. Chem. Phys.* **1955**, *23*, 1833.
(37) Besler, B. H.; Merz, K. M., Jr.; Kollman, P. A. *J. Comput. Chem.* **1990**, *11*, 431.
(38) Singh, U. C.; Kollman, P. A. *J. Comput. Chem.* **1984** *5*, 129.
(39) Breneman, C. M.; Wiberg, K. B. *J. Comput. Chem.* **1990**, *11*, 361.
(40) Yamato, T.; Niimura, N.; Go, N. *Proteins*: *Struct., Funct., Genet.* **1998**, *32*, 268.
(41) Genick, U. K.; Devanathan, S.; Meyer, T. E.; Canestrelli, I. L.; Williams, E.; Cusanovich, M. A.; Tollin, G.; Getzoff, E. D. *Biochemistry* **1997**, *36*, 8.
(42) Düx, G.; Rubinstenn, P.; Vuister, G. W.; Boelens, R.; Mulder, F. A. A.; Hård, K.; Hoff, W. D.; Kroon, A. R.; Crielaard, W.; Hellingwerf, K. J.; Kaptein, R. *Biochemistry* **1998**, *37*, 12689.
(43) He, Z.; Martin, C. H.; Freed, K. F. To be pulished.
(44) Bartlett, R. J.; Silver, D. M. *Int. J. Quantum. Chem.* **1974**, *S8*, 271.
(45) Binkley, J. S.; Pople, J. A. *Int. J. Quantum. Chem.* **1975**, *9*, 229.
(46) Bartlett, R. J.; Purvis, G. D. *J. Chem. Phys.* **1978**, *68*, 2114.
(47) Krishnan, R.; Frisch, M. J.; Pople, J. A. *J. Chem. Phys.* **1980**, *72*, 4244.
(48) Widmark, P.-O.; Malmqvist, P.-A.; Roos, B. O. *Theor. Chim. Acta* **1990**, *77*, 291.
(49) Lorentzon, J.; Malmqvist, P.-A.; Fulscher, M.; Roos, B. O. *Theor. Chim. Acta* **1995**, *91*, 91.